Bilayer graphene spectral function in the random phase approximation and self-consistent GW approximation

Andro Sabashvili, Stellan Östlund, and Mats Granath
Department of Physics, University of Gothenburg, SE-41296 Gothenburg, Sweden
(Received 28 March 2013; revised manuscript received 16 August 2013; published 29 August 2013)

We calculate the single-particle spectral function for doped bilayer graphene in the low energy limit, described by two parabolic bands with zero band gap and long range Coulomb interaction. Calculations are done using thermal Green's functions in both the random phase approximation (RPA) and the fully self-consistent GW approximation. Consistent with previous studies RPA yields a spectral function which, apart from the Landau quasiparticle peaks, shows additional coherent features interpreted as plasmarons, i.e., composite electron-plasmon excitations. In the GW approximation the plasmaron becomes incoherent and peaks are replaced by much broader features. The deviation of the quasiparticle weight and mass renormalization from their noninteracting values is small which indicates that bilayer graphene is a weakly interacting system. The electron energy loss function, $\mathrm{Im}[-\epsilon_q^{-1}(\omega)]$ shows a sharp plasmon mode in RPA which in the GW approximation becomes less coherent and thus consistent with the weaker plasmaron features in the corresponding single-particle spectral function.

DOI: 10.1103/PhysRevB.88.085439 PACS number(s): 73.22.Pr, 71.15.−m, 71.18.+y, 71.45.Gm

I. INTRODUCTION

Since its fabrication, graphene[1–5] has been of interest for both theoreticians and experimentalists. It is a two-dimensional (2D) crystal with carbon atoms arranged on a honeycomb lattice with two sublattices. Due to its unique properties (e.g., high mobility even in highly doped cases) it opens new perspectives for engineering and is a candidate material for future nanoelectronic and spintronic devices.[6]

The subject of this paper is the closely related bilayer graphene, formed by stacking two graphene layers in Bernal "AB" stacking sequence in which the two layers are rotated by 60 degrees. These are coupled by interlayer tunneling with the hopping parameter $t_\perp \approx 0.39$ eV.[7]

Bilayer graphene shares some features with both graphene and the ordinary two-dimensional electronic gas (2DEG). Its dispersion is quadratic, similar to a 2DEG but the effective Hamiltonian is chiral with zero band gap as in the case of graphene.[7,8] In both single layer and bilayer graphene the charge carrier density can be controlled by application of a gate voltage, a fundamental effect for potential technological applications.[1,9] In addition, for bilayer graphene even the band gap is tunable with great potential for device applications.[9,10]

In contrast to single layer graphene the coupling parameter of bilayer graphene is a function of carrier density, $r_s \sim n^{-1/2}$.[2] Thus the strength of Coulomb interaction is tunable, while the coupling parameter for the single layer graphene is a constant and lies in the interval $0 \leqslant r_s \lesssim 2.2$. By comparing the values of r_s for single and bilayer graphene ($r_s \approx 68.5 \times 10^5/\sqrt{n}$, where n is the number of carriers per cm^{-2} with $n \approx 10^9 - 5 \times 10^{12}$) in vacuum it is clear that the strength of the Coulomb interaction can be much larger in bilayer graphene.[2]

The electronic structure of bilayer graphene[7,11] is characterized by the single particle spectral function $A(\vec{k},\omega)$, which can be measured experimentally by angle resolved photoemission spectroscopy (ARPES).[12,13] It obeys the sum rule $\int \frac{d\omega}{2\pi} A(\vec{k},\omega) = 1$ and can be interpreted as the probability distribution of an electron having momentum $\vec{k}$ and energy ω. Sensarma *et al.*[14] studied how Coulomb interaction affects the single particle spectral function of bilayer graphene away from half filling. These authors used the RPA to show that doped bilayer graphene is a Fermi liquid in the low energy limit, with a sharp quasiparticle peak. They also found additional weaker peak structures that they interpreted as plasmarons; a quasiparticle formed by the coupling between electron and plasmon, as originally predicted by B. I. Lundqvist.[15] Earlier RPA studies of undoped bilayer graphene found a marginal Fermi liquid with linear in ω decay rate related to the finite density of interband excitations down to low energies.[16,17] In addition, it has been shown that at charge neutrality bilayer graphene reveals instabilities to various broken-symmetry phases.[18–23] Studying the physics of interaction between electrons and plasmons in graphene is particularly interesting because of recently proposed "plasmonic" devices that could merge photonics and electronics.[13]

Experimentally, plasmarons in the single layer graphene were observed by A. Bostwick *et al.*[13] using angle-resolved photoemission spectroscopy. Apart from the two single particle crossing bands, two additional bands were observed and interpreted as a spectrum of plasmarons. The experimentally measured spectral function is similar to that obtained within RPA.[24,25]

In this paper we compute numerically the single-particle spectral function $A(\vec{k},\omega)$ for doped bilayer graphene in the low energy two-band approximation in both RPA and the fully self-consistent GW approximation.[26–28] We use a recently developed thermal Green's function formalism, based on a finite set of imaginary frequencies and analytic continuation to real frequencies for the single-particle Green's functions.[29]

The results, presented in Fig. 1, show the spectral function with long lived Landau quasiparticles and satellite plasmaron peaks in RPA [Fig. 1(a)] and confirm the results of analytic calculations,[7,14,30] whereas in the GW approximation the plasmaron peaks are replaced by broad shoulders [Fig. 1(b)]. It has been emphatically argued that self-consistent GW underestimates the coherence of collective excitations[28,31–33]

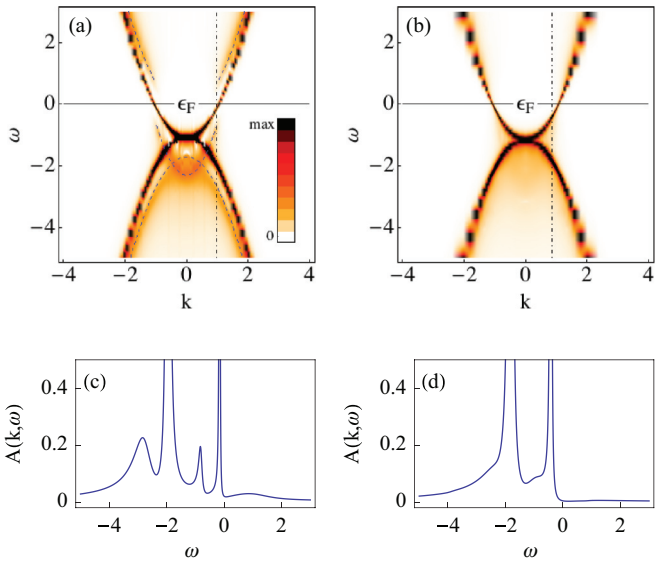

FIG. 1. (Color online) Single particle spectral function for bilayer graphene in the low energy limit at $r_s = 3$. (a) RPA, (b) GW. The bare bands $\epsilon_{\vec{k}} = \pm k^2$ (in units $k_F = 1, \epsilon_F = 1$) are rotationally symmetric (the patchy appearance is due to the finite k-space resolution). (c) and (d) are the cuts (dash-dotted lines) in (a) and (b), respectively. Dashed lines are guides to the eye for plasmaron dispersions.

and our results showing a marked difference between the satellite peaks in RPA and GW most likely agree with this. Nevertheless we argue that the GW results are valuable as a benchmark for more sophisticated self-consistent approaches including vertex corrections to the polarization. Below we describe our calculations in more detail.

II. GW APPROXIMATION

The GW approximation is derived perturbatively from the Hedin's equations,[26,27] giving the self-energy

$$\Sigma^{GW}_{\vec{k}}(i\omega_n) = \frac{1}{\beta}\int \frac{d^2q}{(2\pi)^2}\sum_{m=-\infty}^{\infty} W_{\vec{q}}(i\omega_m)G_{\vec{k}-\vec{q}}(i\omega_n - i\omega_m), \tag{1}$$

where $W_{\vec{q}}(i\omega_n)$ and $G_{\vec{k}}(i\omega_n)$ are the dressed interaction and Green's function, respectively (all quantum numbers, such as momentum, spin, etc., are incorporated in $\vec{k}$ and $\vec{q}$). The argument of the Green's function is the fermionic Matsubara frequency $\omega_n = (2n+1)\pi/\beta$, and the dressed interaction is a function of the bosonic Matsubara frequency $\omega_m = 2\pi m/\beta$ with m integer. After computing $\Sigma^{GW}_{\vec{k}}(i\omega_n)$ (first diagram in Fig. 2) one should, in general, add the Hartree diagram (second diagram in Fig. 2) to it which in the case of long-

FIG. 2. Contribution to the self-energy from the GW approximation and Hartree diagram. Double wiggly line, single wiggly line, and double line correspond to dressed interaction, bare interaction, and dressed Green's function, respectively.

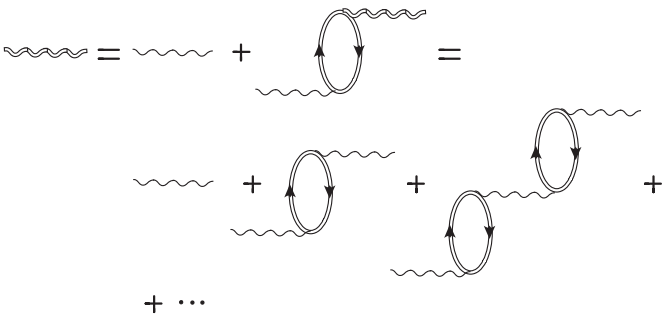

FIG. 3. Screened interaction in the GW approximation is given by geometric series. Bubble diagram represents polarization $\Pi_{\vec{q}}(i\omega_n)$.

range Coulomb interaction gives zero contribution because it is canceled by the positive background charge.[34] The approximation has the same form as the standard Hartree-Fock (HF) approximation but the latter uses the bare Green's function and interaction, while the former is based on the dressed Green's function $G_{\vec{k}}(\omega)$ and dynamically screened (dressed) interaction.

The screened interaction $W_{\vec{q}}(i\omega_n)$ is an infinite geometric series of diagrams (Fig. 3) consisting of the bare interaction V_q and the irreducible polarization diagram $\Pi_{\vec{q}}(i\omega_n)$ which in GW is given by

$$\Pi_{\vec{q}}(i\omega_n) = -g\int \frac{d^2k}{(2\pi)^2}\frac{1}{\beta}\sum_{m=-\infty}^{\infty} G_{\vec{k}}(i\omega_m)G_{\vec{k}+\vec{q}}(i\omega_n + i\omega_m), \tag{2}$$

where g is the degeneracy factor. In RPA it is computed using the same relation but with the full Green's functions replaced by the bare ones. So, the RPA polarization is just the zeroth order term in the expansion of $\Pi_{\vec{q}}(\omega_n)$ in the bare interaction. After summing up the geometric series one obtains the following expression for the screened interaction

$$W_{\vec{q}}(i\omega_n) = \frac{V_q}{1 + V_q\Pi_{\vec{q}}(i\omega_n)}. \tag{3}$$

The effective bare Coulomb interaction for bilayer graphene is given by $V_q = \frac{2\pi e^2}{\kappa q}$ where κ represents the background dielectric constant.[11] Using E_F and k_F as units of energy and momentum, respectively, enables us to write V_q in terms of the dimensionless coupling parameter $r_s = e^2 gm/(k_F\kappa)$:

$$V_q = \frac{\pi r_s}{q}. \tag{4}$$

III. BILAYER GRAPHENE

A. Effective model

The low energy two-band approximation in bilayer graphene[7,35] is valid if the scale of all relevant energies is smaller than the interlayer hopping parameter $t_\perp$ and the doping is sufficiently small.[2,36] It has been shown that in order to explain the characteristics of some quantities (e.g., compressibility) taking into account all four bands is necessary.[36–39] Since we are studying the low energy properties we focus on the two-band approximation where the two outer bands can be ignored and thus the four-band model is reduced

to the effective two-band model with the total degeneracy of $g = 4$ (due to the spin and valley index) given by

$$H_0 = -\frac{1}{2m}\begin{pmatrix} 0 & (k_x + ik_y)^2 \\ (k_x - ik_y)^2 & 0 \end{pmatrix}. \tag{5}$$

It is clear that the corresponding energy spectrum is parabolic,

$$\epsilon_k = \pm\frac{k^2}{2m}, \tag{6}$$

where $m = t_\perp/(2v_F^2) \approx 0.054m_e$ is the effective mass of the electron in the low energy limit with m_e being the free electron mass. The corresponding free fermionic Matsubara Green's function is

$$\hat{G}^0_{\vec{k}}(i\omega_n) = (i\omega_n - H_0 + \mu)^{-1} = \frac{1}{2}\sum_{s=\pm}\frac{1 + s\hat{\sigma}_{\vec{k}}}{i\omega_n - s|\epsilon_k| + \mu}, \tag{7}$$

s indexes the conduction and valence bands, μ is the chemical potential, and $\sigma_{\vec{k}}$ is given by

$$\hat{\sigma}_{\vec{k}} = \sum_{j=\pm}\frac{k_j^2}{k^2}\hat{\sigma}_j = \sum_{j=\pm} e^{j2\theta_{\vec{k}}}\hat{\sigma}_j. \tag{8}$$

Here we have defined $k_\pm = k_x \pm ik_y$, $\hat{\sigma}_\pm = (\hat{\sigma}_1 \pm i\hat{\sigma}_2)/2$, $\hat{\sigma}_1$ and $\hat{\sigma}_2$ are Pauli matrices, and $\theta_{\vec{k}}$ is the angle of the vector $\vec{k}$ with respect to the x axis.

Let us rewrite Eq. (2) for the two-band model. After summing over all internal indices we obtain the following expression for $\Pi_{\vec{q}}(i\omega_n)$,

$$\Pi_{\vec{q}}(i\omega_n) = -\frac{g}{\beta}\int\frac{d^2k}{(2\pi)^2}\sum_{m=-\infty}^{\infty}\mathrm{Tr}(\hat{G}_{\vec{k}}(i\omega_m) \times \hat{G}_{\vec{k}+\vec{q}}(i\omega_n + i\omega_m)). \tag{9}$$

In the noninteracting limit $\Pi_{\vec{q}}(i\omega_n)$ can be written in the following simple form:

$$\Pi^0_{\vec{q}}(i\omega_n) = -g\sum_{s,s'}\int\frac{d^2k}{(2\pi)^2}\frac{(f^s_k - f^{s'}_{k+q})F_{s,s'}(\vec{k},\vec{k}+\vec{q})}{i\omega_n + s|\epsilon_k| - s'|\epsilon_{k+q}| + \mu}, \tag{10}$$

where $f^s_k = 1/(1 + e^{\beta(s|\epsilon_k|-\mu)})$ is the Fermi distribution function and

$$F_{s,s'}(\vec{k},\vec{k}+\vec{q}) = \tfrac{1}{4}\mathrm{Tr}(1 + s\hat{\sigma}_{\vec{k}})(1 + s'\hat{\sigma}_{\vec{k}+\vec{q}}) = \tfrac{1}{2}(1 + ss'\cos(2\theta_{\vec{k},\vec{k}+\vec{q}})),$$

with $\theta_{\vec{k},\vec{k}+\vec{q}}$ being the angle between the vectors $\vec{k}$ and $\vec{k}+\vec{q}$. $\Pi_{\vec{q}}(i\omega_n)$ is an angle-independent function which can be seen by extracting the angle $\theta_{\vec{q}}$ using the rotation of the integration variable in Eq. (9) with $\theta_{\vec{q}}$. Consequently, the screened interaction is angle independent as well. Note that since the polarization is a scalar due to the trace in Eq. (9) the screened interaction remains to be a scalar quantity as well.

The GW self-energy is generalized to

$$\hat{\Sigma}^{GW}_{\vec{k}}(i\omega_n) = \frac{1}{\beta}\int\frac{d^2q}{(2\pi)^2}\sum_{m=-\infty}^{\infty}W_q(i\omega_m)\hat{G}_{\vec{k}-\vec{q}}(i\omega_n - i\omega_m). \tag{11}$$

After performing the following integration variable transformations in Eq. (11) with $\hat{G}_{\vec{k}-\vec{q}}$ replaced by $\hat{G}^0_{\vec{k}-\vec{q}}$,

$$\vec{q}_1 = \vec{k} - \vec{q} \tag{12}$$

and

$$\vec{q}_2 = \mathcal{R}(\pi + \theta_{\vec{k}})\vec{q}_1, \tag{13}$$

where $\mathcal{R}(\pi + \theta_{\vec{k}})$ denotes the rotation matrix with the angle $\pi + \theta_{\vec{k}}$ one can see that $\hat{\Sigma}^{GW}_{\vec{k}}(i\omega_n)$ and consequently the fully interacting Green's function $\hat{G}_{\vec{k}}(i\omega_n)$ have and retain the same structure as that of the free Green's function [Eqs. (14) and (15)] throughout the whole self-consistent calculation.[40]

$$\hat{G}^0_{\vec{k}}(i\omega_n) = \frac{1}{2}\begin{pmatrix} a^+_k & a^-_k e^{i2\theta_{\vec{k}}} \\ a^-_k e^{-i2\theta_{\vec{k}}} & a^+_k \end{pmatrix} \tag{14}$$

$$a^\pm_k \equiv (i\omega_n - |\epsilon_k| + \mu)^{-1} \pm (i\omega_n + |\epsilon_k| + \mu)^{-1}. \tag{15}$$

So, it is sufficient to set up calculations for $\hat{\Sigma}^{GW}_{\vec{k}}(i\omega_n)$ and $\hat{G}_{\vec{k}}(i\omega_n)$ only at $\theta_{\vec{k}} = 0$.

B. Periodized Green's functions

The GW approximation implies a self-consistent numerical calculation, which may be solved iteratively.[41] Obviously these calculations include very demanding operations including infinite sums over Matsubara frequencies. In order to cope in numerical calculations with these kinds of problems we use a formalism for finite temperature fermionic thermal Green's functions in the single band case described in Ref. 29 and summarized below.

Performing numerical calculations using thermal Green's functions[42,43] may be done by the discretization of imaginary time. Since the fermionic thermal Green's function is antiperiodic over $\tau \in [-\beta,\beta]$ domain with the period β we discretize the interval $\tau \in [0,\beta]$ into N evenly spaced points, $\tau = (\beta/N)j, j = 1,\ldots,N-1$. Due to the discontinuity of the fermionic Green's function at $\tau = 0$ (limits $\tau \to 0^-$ and $\tau \to 0^+$ differ from each other) some specific value must be assigned to $G_k(\tau_j = 0)$ when doing numerical computations. We define $G_k(\tau_j = 0)$ by the average of $G_k(\tau = 0^-)$ and $G_k(\tau = 0^+)$. After applying discrete Fourier transformation to the noninteracting thermal Green's function

$$G^0_k(\tau) = e^{-\epsilon_k\tau}[(n_k - 1)\theta(\tau) + n_k\theta(-\tau)], \tag{16}$$

where $n_k = \langle c^\dagger_k c_k\rangle$ is the occupation number we obtain periodic set of the Green's function values in the Matsubara frequency space

$$G^0_k(i\omega_n) = \eta\coth\eta(i\omega_n - \epsilon_k). \tag{17}$$

Here $\eta \equiv \frac{\beta}{2N}$ and ϵ_k is a single-particle excitation spectrum for a given model. It is obvious that Eq. (17) is periodic under $i\omega_n \to i\omega_n + i\Omega_N, \Omega_N \equiv \frac{\pi}{\eta}$. The periodized full Green's function is given by

$$G_k(i\omega_n) = \eta\coth\eta(i\omega_n - \epsilon_k - \Sigma_k(i\omega_n)), \tag{18}$$

which has the correct noninteracting limit and together with $G_k^0(i\omega_n)$ yields standard continuum expression for the Greens function as N tends to $\infty(\eta \to 0)$. Due to the nontrivial hyperbolic function in Eq. (18) one can not define the self-energy using simply G_0^{-1} and G^{-1} as is done in the standard theory. In this case the self-energy is defined by the amputated skeleton diagrams (Ref. 42, see Sec. 5.1) and through Eq. (18).

In the case of the two band model $G_k(i\omega_n)$ is generalized to

$$\hat{G}_{\vec{k}}(i\omega_n) = \eta \coth \eta \left(\left(\hat{G}^0_{\vec{k}}(i\omega_n) \right)^{-1} - \hat{\Sigma}_{\vec{k}}(i\omega_n) \right), \qquad (19)$$

where

$$\left(\hat{G}^0_{\vec{k}}(i\omega_n) \right)^{-1} = \begin{pmatrix} i\omega_n + \mu & -|\epsilon_k|\, e^{i2\theta_{\vec{k}}} \\ -|\epsilon_k|\, e^{-i2\theta_{\vec{k}}} & i\omega_n + \mu \end{pmatrix} = (i\omega_n + \mu) - |\epsilon_k| \hat{\sigma}_{\vec{k}}.$$

The periodized Green's function for both single and two-band cases is consistent with the corresponding Luttinger-Ward Γ-functional[44,45] [the former is consistent with the Γ-functional as presented in Eq. (4) in Ref. 29 while the latter with the same equation where $G_k(i\omega_n)$ is replaced by $\hat{G}_{\vec{k}}(i\omega_n)$].

To perform analytic continuation for $G_k(i\omega_n)$ we first rewrite it by means of a conformal transformation in a new basis where it can be represented as a sum of simple poles. Then the Padé method[46] of fitting to a rational function is used which enables us to evaluate the Green's function on the real frequency axis. In the case of a two-band model the trace of $\hat{G}_{\vec{k}}(i\omega_n)$ is used as an input to the same procedure of analytic continuation as the one carried out for $G_k(i\omega_n)$.

We start the self-consistent calculation by discretizing momenta and angles. Since our interest is focused on the low energy properties the finite range of $|\vec{k}|(|\vec{k}| \in [0,4])$ is discretized into 40 points logarithmically giving a denser number of points around k_F. The rest of the integration variables ($|\vec{q}|$, $\theta_{\vec{k}}$, and $\theta_{\vec{q}}$) are discretized linearly. $|\vec{q}|$ is discretized into 80 points and lies in the interval $[1/80, 4]$ while the number of discretization points for $\theta_{\vec{k}}$ and $\theta_{\vec{q}}$ is 10. First, the free Greens's function is evaluated at $\theta_{\vec{k}} = 0$ and then it is rotated by an angle $\theta_{\vec{k}}$ in order to obtain the polarization [Eq. (9)]. Then the screened interaction is computed using Eq. (3) which enables us to evaluate the GW self-energy [Eq. (11)]. After calculating $\hat{\Sigma}^{GW}_{\vec{k}}(i\omega_n)$ at $\theta_{\vec{k}} = 0$ we update the Green's function through Eq. (19). This is done repeatedly: If the procedure converges to a fixed point, a solution has been found. The calculations are done at $T/\epsilon_F = 1/10$ with $N = 121$ number of Matsubara frequencies.

C. Spectral function

The spectral function is given by

$$A(\vec{k},\omega) = -\tfrac{1}{\pi} \mathrm{Im}[\mathrm{Tr} \hat{G}_{\vec{k}}(\omega + i0^+)], \qquad (20)$$

where we perform analytic continuation after applying trace to $\hat{G}_{\vec{k}}(i\omega_n)$. In order to study the low energy properties we also compute the spectral function projected on the conduction band

$$A^+(\vec{k},\omega) = -\frac{1}{\pi} \mathrm{Im}[G_{\vec{k}}(s = +, \omega + i0^+)], \qquad (21)$$

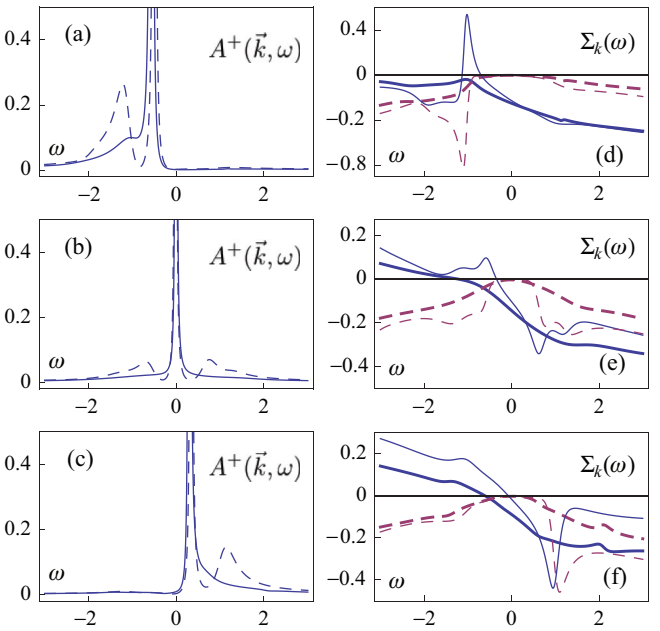

FIG. 4. (Color online) $r_s = 3$. Left column: spectral weight in RPA (dashed line) and GW approximation (solid line) at $k \approx 0.76k_F$ (a), $k = k_F^*$ (b), $k \approx 1.20k_F$ (c). Right column: the real (blue solid line) and imaginary (red dashed line) part of the self-energy at $k \approx 0.76k_F$ (d), $k = k_F^*$ (e), $k \approx 1.20k_F$ (f) in RPA (thin line) and GW approximation (thick line).

where $G_{\vec{k}}(s = +,\omega)$ represents the eigenvalue of $\hat{G}_{\vec{k}}(i\omega_n)$ corresponding to the upper band after analytic continuation to the real axis. Spectral weight conservation is equivalent to $\int d\omega A(\vec{k},\omega) = 2$ and $\int d\omega A^+(\vec{k},\omega) = 1$, respectively.

In Figs. 4 and 5 we present the spectral functions (left column) for different values of k together with the corresponding self-energies (right column) in the GW approximation and RPA at $r_s = 3$ and $r_s = 7$ corresponding to the carrier densities $n = 3 \times 10^{12}\mathrm{cm}^{-2}$ and $n = 6 \times 10^{11}\mathrm{cm}^{-2}$ for SiO_2 substrate, respectively. Due to the interaction k_F is slightly shifted because of the finite value of $\mathrm{Re}\Sigma_{k_F}(\omega = 0)$ (see blue solid curves in the right panels of Figs. 4 and 5). The spectral functions in Figs. 4(b) and 5(b) are computed at k_F^* which is different from the noninteracting Fermi momentum, $k_F = 1$.

As the plots show the spectral weight in the RPA away from k_F has two peaks: the main Landau quasiparticle peak and plasmaron peaks. The presence of the plasmaron excitation also give jumps in the real and imaginary parts of the corresponding self-energies. The RPA plasmaron excitation has lower weight at $r_s = 7$ than the one at $r_s = 3$, although the spectral functions have qualitatively the same behavior which is also noticeable in the case of the GW approximation. Most of the structure obtained in the RPA is not presented in the GW approximation. We interpret this as being due to stronger screening in GW.

We also compute the electron energy loss spectrum $\mathrm{Im}[-\epsilon_q^{-1}(\omega)]$, where $\epsilon_q(\omega)$ is the dielectric function and is given by

$$\epsilon_q(\omega) = 1 + V_q \Pi_{\vec{q}}(\omega). \qquad (22)$$

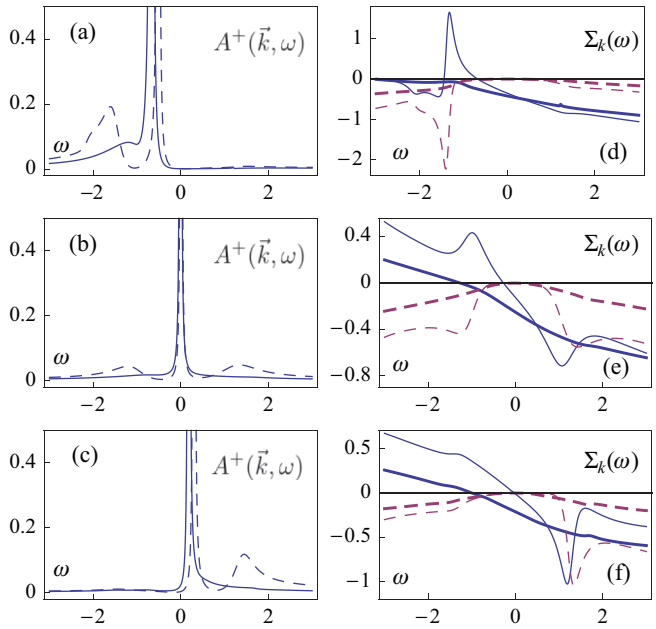

FIG. 5. (Color online) $r_s = 7$. Left column: spectral weight in RPA (dashed line) and GW approximation (solid line) at $k \approx 0.76k_F$ (a), $k = k_F^*$ (b), $k \approx 1.20k_F$ (c). Right column: the real (blue solid line) and imaginary (red dashed line) part of the self-energy at $k \approx 0.76k_F$ (d), $k = k_F^*$ (e), $k \approx 1.20k_F$ (f) in RPA (thin line) and GW approximation (thick line).

In Fig. 6(a) $\mathrm{Im}[-\epsilon_q^{-1}(\omega)]$ in RPA is plotted showing the plasmaron dispersion relation (black color) which is in quite good agreement for small q values with its analytic form (solid line) expanded up to second order in q,[2,30]

$$\omega_q \simeq e\sqrt{\frac{g\epsilon_F q}{\kappa}}\left(1 - \frac{r_s q}{8k_F}\right).$$

$\mathrm{Im}[-\epsilon_q^{-1}(\omega)]$ was also calculated in the GW approximation [Fig. 6(b)] where the plasmon mode is less coherent than that in RPA which is in agreement with the fact that the plasmaron features in the GW spectral function are weaker than in RPA.

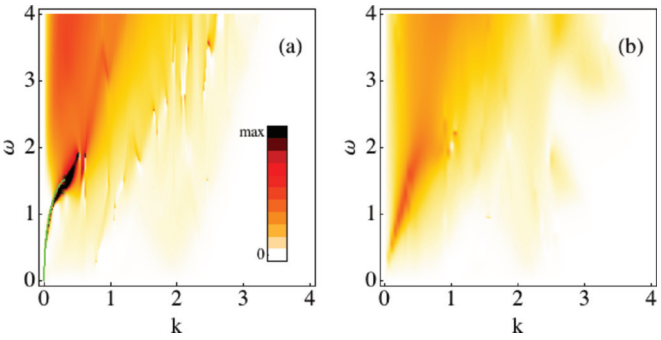

FIG. 6. (Color online) $\mathrm{Im}[-\epsilon_q^{-1}(\omega)]$ in RPA (a) and GW approximation (b) at $r_s = 7$ (same color intensity scale on both plots). Green solid line in (a) represents the plasmon dispersion expanded up to the second order in q. The unexpected discontinuities are artificial and due to difficulties with the analytic continuation of a two-particle function.

TABLE I. Quasiparticle weight Z and effective mass relative to the one of the free electron m^*/m.

	$r_s = 3$		$r_s = 7$	
	Z	$\frac{m^*}{m}$	Z	$\frac{m^*}{m}$
RPA	0.798	0.978	0.685	0.986
GW	0.851	0.946	0.806	0.929

D. Quasiparticle weight and effective mass

The quasiparticle weight Z for conduction band and renormalized mass m^*, given in Table I, are computed for both the GW and RPA approximations using the formulas:

$$Z = \frac{1}{1 - \frac{\partial \mathrm{Re}\Sigma_{k_F}(\omega)}{\partial\omega}\Big|_{\epsilon_F}}, \tag{23}$$

$$\frac{m^*}{m} = \frac{Z^{-1}}{1 + \frac{m}{k_F}\frac{\partial \mathrm{Re}\Sigma_k(\omega=\epsilon_F)}{\partial k}\Big|_{k_F}}. \tag{24}$$

As expected, the quasiparticle weight decreases with increasing interaction strength because the interaction shifts the weight from the coherent quasiparticle peak through incoherent scattering. Since the GW approximation does not yield the plasmaron peaks and the interaction gets more screened, most of the weight is concentrated in the Landau quasiparticle which results in a bigger quasiparticle weight than that in the case of RPA. The mass renormalization is less than 7% in both approximations meaning that we are dealing with a weakly interacting system.

By comparing our results with the ones presented in Refs. 14 and 47 one can see that the agreement is quite good. In Ref. 47 the screening is taken into account through the Thomas-Fermi approximation and mass renormalization is computed for different magnitudes of the screening. The agreement between our results and those presented in Ref. 47 is very good when the Thomas-Fermi screening is not reduced.

IV. CONCLUSION

We present the single particle spectral function and self-energy for bilayer graphene in the low energy limit as described with a two band model. Calculations are done in both RPA and self-consistent GW using a discretized thermal Green's function formalism. In RPA, the spectral function and energy loss spectrum show prominent plasmaron peaks and a sharp plasmon mode, respectively, which together with quasiparticle weight and effective mass are in good agreement with those computed using a conventional Matsubara Green's function method.[14] In GW the plasmaron peaks are replaced by broad shoulders which is consistent with the observation of a less coherent plasmon mode. Further studies, including experiments, should elucidate to what extent GW underestimates (or RPA overestimates) the coherent nature of the excitations. Independently of the graphene physics the calculations show that the periodized Green's function formalism[29] is an efficient method for self-consistent calculations.

ACKNOWLEDGMENTS

We acknowledge useful discussions with J. Nilsson and R. Sensarma. This work was supported by MP^2 platform at the University of Gothenburg and Swedish Research Council (Grant Nos. 2011-4054 and 2008-4242).

[1] K. S. Novoselov, A. K. Geim, S. V. Morozov, D. Jiang, Y. Zhang, S. V. Dubonos, I. V. Grigorieva, and A. A. Firsov, Science **306**, 666 (2004).

[2] S. Das Sarma, Sh. Adam, E. H. Hwang, and E. Rossi, Rev. Mod. Phys **83**, 407 (2011).

[3] A. H. Castro Neto, F. Guinea, N. M. R. Peres, K. S. Novoselov, and A. K. Geim, Rev. Mod. Phys. **81**, 109 (2009).

[4] J. W. McClure, Phys. Rev. **108**, 612 (1957).

[5] P. R. Wallace, Phys. Rev. **71**, 622 (1947).

[6] A. K. Geim and K. S. Novoselov, Nat. Mater. **6**, 183 (2007).

[7] V. N. Kotov, B. Uchoa, V. M. Pereira, F. Guinea, and A. H. Castro Neto, Rev. Mod. Phys. **84**, 1067 (2012).

[8] M. Lv and Sh. Wan, Phys. Rev. B **81**, 195409 (2010).

[9] T. Ohta, A. Bostwick, Th. Seyller, K. Horn, and E. Rotenberg, Science **313**, 951 (2006).

[10] E. V. Castro, K. S. Novoselov, S. V. Morozov, N. M. R. Peres, J. M. B. Lopes dos Santos, J. Nilsson, F. Guinea, A. K. Geim, and A. H. Castro Neto, Phys. Rev. Lett. **99**, 216802 (2007).

[11] J. Nilsson, A. H. Castro Neto, N. M. R. Peres, and F. Guinea, Phys. Rev. B **73**, 214418 (2006).

[12] A. Bostwick, T. Ohta, T. Seyller, K. Horn, and E. Rotenberg, Nat. Phys. **3**, 36 (2007).

[13] A. Bostwick, F. Speck, Th. Seyller, K. Horn, M. Polini, R. Asgari, A. H. MacDonald, and E. Rotenberg, Science **328**, 999 (2010).

[14] R. Sensarma, E. H. Hwang, and S. Das Sarma, Phys. Rev. B **84**, 041408(R) (2011); **86**, 079912(E) (2012).

[15] B. I. Lundqvist, Phys. kondens. Materie **6**, 193 (1967).

[16] Y. Barlas and K. Yang, Phys. Rev. B **80**, 161408(R) (2009).

[17] R. Nandkishore and L. Levitov, Phys. Rev. B **82**, 115431 (2010).

[18] H. Min, G. Borghi, M. Polini, and A. H. MacDonald, Phys. Rev. B **77**, 041407(R) (2008).

[19] O. Vafek and K. Yang, Phys. Rev. B **81**, 041401 (2010).

[20] F. Zhang, H. Min, M. Polini, and A. H. MacDonald, Phys. Rev. B **81**, 041402 (2010).

[21] Y. Lemonik, I. Aleiner, and V. I. Fal'ko, Phys. Rev. B **85**, 245451 (2012).

[22] M. Kharitonov, Phys. Rev. Lett. **109**, 046803 (2012).

[23] M. Kharitonov, Phys. Rev. B **86**, 195435 (2012).

[24] E. H. Hwang and S. Das Sarma, Phys. Rev. B **77**, 081412 (2008).

[25] M. Polini, R. Asgari, G. Borghi, Y. Barlas, T. Pereg-Barnea, and A. H. MacDonald, Phys. Rev. B **77**, 081411 (2008).

[26] L. Hedin, Phys. Rev. **139**, A796 (1965).

[27] L. Hedin and S. Lundqvist, *Solid State Physics*, edited by H. Ehrenreich, F. Seitz, and D. Turnbull (Academic Press, New York, 1969), Vol. 23.

[28] F. Aryasetiawany and O. Gunnarsson, Rep. Prog. Phys. **61**, 237 (1998).

[29] M. Granath, A. Sabashvili, H. U. R. Strand, and S. Östlund, Ann. Phys. **524**, 147 (2012).

[30] R. Sensarma, E. H. Hwang, and S. Das Sarma, Phys. Rev. B **82**, 195428 (2010).

[31] U. von Barth and B. Holm, Phys. Rev. B **54**, 8411 (1996).

[32] B. Holm and U. von Barth, Phys. Rev. B **57**, 2108 (1998).

[33] T. Ayral, Ph. Werner, and S. Biermann, Phys. Rev. Lett. **109**, 226401 (2012).

[34] Richard. D. Mattuck, *A guide to Feynman diagrams in the many-body problem*, 2nd ed. (Dover Publications, New York, 1992).

[35] E. McCann and V. I. Fal'ko, Phys. Rev. Lett. **96**, 086805 (2006).

[36] G. Borghi, M. Polini, R. Asgari, and A. H. MacDonald, Phys. Rev. B **80**, 241402 (2009).

[37] G. Borghi, M. Polini, R. Asgari, and A. H. MacDonald, Phys. Rev. B **82**, 155403 (2010).

[38] S. V. Kusminskiy, J. Nilsson, D. K. Campbell, and A. H. Castro Neto, Phys. Rev. Lett. **100**, 106805 (2008).

[39] S. V. Kusminskiy, D. K. Campbell, and A. H. Castro Neto, Europhys. Lett. **85**, 58005 (2009).

[40] A. Sabashvili, Ph. D. thesis, University of Gothenburg, 2013.

[41] Note that forward iteration is not always an optimal method for self-consistent calculations. In some cases it is unable to find all fixed points and more advanced techniques are required. See, e.g., H. U. R. Strand, A. Sabashvili, M. Granath, B. Hellsing, and S. Östlund, Phys. Rev. B **83**, 205136 (2011).

[42] J. W. Negele and H. Orland, *Quantum Many-Particle Systems* (Addison-Wesley, New York, 1988).

[43] A. A. Abriksov, L. P. Gorkov, and I. E. Dzyaloshinskii, *Quantum field theoretical methods in many body physics*, 2nd ed. (Pergamon, Oxford, 1965).

[44] J. M. Luttinger and J. C. Ward, Phys. Rev. **118**, 1417 (1960).

[45] M. Bonitz, R. Nareyka, and D. Semkat, *Progress in nonequilibrium Green's functions, Proceedings of the conference, "Kadanoff-Baym Equations Progress and Perspectives for Many-body Physics", Rostock Germany, 20–24 September, 1999* (World Scientific, Singapore, 2000).

[46] H. J. Vidberg and J. W. Serene, J. Low Temp. Phys. **29**, 179 (1977).

[47] G. Borghi, M. Polini, R. Asgari, and A. H. MacDonald, Solid State Commun. **149**, 1117 (2009).